中正嶺學報 第三十四卷 第二期 民國 95.5.
JOURNAL OF C.C.I.T., VOL.34, NO.2, MAY, 2006

短文 Short Note

Sensitivity Analysis of MEMS Force Sensor Beam on the Test Chip

Feng-I Chang
Center for General Education, Tzu-Hui institute of technology

ABSTRACT

In this paper, we study the micro-electro-mechanical system (MEMS) with a force sensor beam's sensitivity. According to the analysis, each mode has a different sensitivity and the first mode is the most sensitive mode of MEMS force sensor beam on the test chip. As the spring constant increases, the fifth vibration mode is more sensitive than the other modes. Furthermore, the spring constant has a significant effect on the sensitivity of the MEMS force sensor beam, and this should note when designing new the MEMS force sensor beam on the test chip.
Keywords: MEMS, sensitivity, force sensor beam, chip

在測試晶片上微機電系統力感測樑的敏感性分析

張豐宜
慈惠醫護管理專科學校通識教育中心

摘要

在這篇論文，我們研究這微機電系統和一個力的感測樑的敏感性分析。根據分析，在這測試晶片上微機電系統力感測樑的第一個模式是較敏感的和每個模式有不同的敏感性。當彈簧常數增加，這第五個振動模式是較其他模式敏感。而且, 這彈簧常數有一個重要的效應在這個微感測樑的敏感性上，和可以當成設計新的測試晶片上微感測樑的資料。
關鍵字: 微機電系統、敏感性、力感測樑、晶片

文稿收件日期 94.6.16; 文稿修正後接受日期 94.11.11.
Manuscript received June 16, 2005; revised November 11, 2005.

I. INTRODUCTION

The atomic force microscope (AFM) was developed for studied the nature of the surface topography of different samples on a nanometer scale [1,2]. Betzig et al. [3] studied the combined shear force and near-field scanning optical microscopy. Simon et al. [4] obtained the shear-force distance control at megahertz frequencies for near-field scanning optical microscopy. Shalom et al. [5] investigated a micropipette force probe suitable for near-field scanning optical microscopy. Haque et al. [6] improved device design and a new robust fabrication process for cofabrication of a uniaxial tensile sample and a force sensor.

In this paper, the dynamic responses of an MEMS's force sensor beam was considered. The modal sensitivities for force sensor beam vibration was derived, and an approximate solution was obtained using the Laplace Transform method.

II. METHOD OF ANALYSIS

The partial differential equation of the bending vibrations of a force sensor beam with later spring, according to Bernoulli -Euler theory, is the well known expression (see Figure 1)

$$EI\frac{\partial^4 w(x,t)}{\partial x^4}+\rho A\frac{\partial^2 w(x,t)}{\partial t^2}+k_s\delta(x-x_s)w(x,t)=0 \tag{1}$$

where ρ is the volume density, A is the cross-sectional area of force sensor beam, E is the Young's modulus of elasticity of the beam, I is the area moment of inertia of the beam and $\delta(\cdot)$ is the Dirac delta function.

Assume a solution of equation (1) as the form

$$w(x,t)=W(x)e^{i\omega t} \tag{2}$$

Substituting equation (2) into equation (1) gives

$$EIW''''-\rho A\omega^2 W+k_s\delta(x-x_s)W=0 \tag{3}$$

where ω is the natural frequency.
The corresponding boundary conditions are

$$W(0)=0 \quad , \quad W'(0)=0 \tag{4a,b}$$

$$W(L)=0 \quad , \quad W'(L)=0 \tag{4c,d}$$

Take the Laplace transform of equation (3) in conjuction with the boundary condition equations (4a) and (4b), and then apply the inverse Laplace transform yields

$$W(x) = \frac{B}{2\beta^2}(\cosh \beta x - \cos \beta x)$$

$$+ \frac{D}{2\beta^3}(\sinh \beta x - \sin \beta x)$$

$$- \frac{k_s}{2EI} \cdot \frac{1}{\beta^3}[\sinh\beta(x-x_s) - \sin\beta(x-x_s)] \cdot W(x_s) \cdot H(x-x_s) \tag{5}$$

$$\beta = \left(\frac{\rho A \omega^2}{EI}\right)^{\frac{1}{4}} \tag{6}$$

where $B = W''(0)$, $D = W'''(0)$ and $H(\cdot)$ is the Heaviside unit step function. Then substituting equation (5) into the boundary condition equations (4c) and (4d) yields the following two equations

$$\frac{1}{2\beta^2}\{(\cosh(\beta L) - \cos(\beta L)) - \frac{k_s}{2EI\beta^3}[\sinh(\beta(L-x_s)) - \sin(\beta(L-x_s))]$$
$$\cdot (\cosh(\beta x_s) - \cos(\beta x_s))\} B +$$
$$\frac{1}{2\beta^3}\{(\sinh(\beta L) - \sin(\beta L))$$
$$- \frac{k_s}{2EI\beta^3}[\sinh(\beta(L-x_s)) - \sin(\beta(L-x_s))]$$
$$\cdot (\sinh(\beta x_s) - \sin(\beta x_s))\} D = 0 \tag{7}$$

$$\frac{1}{2\beta}\{(\sinh(\beta L) + \sin(\beta L)) - \frac{k_S}{2EI\beta^3}[\cosh(\beta(L-x_S))$$
$$- \cos(\beta(L-x_s))] \cdot (\cosh(\beta x_S) - \cos(\beta x_S))\} B +$$
$$\frac{1}{2\beta^2}\{(\cosh(\beta L) - \cos(\beta L))$$
$$- \frac{k_s}{2EI\beta^3}[\cosh(\beta(L-x_s)) - \cos(\beta(L-x_s))]$$
$$\cdot (\sinh(\beta x_s) - \sin(\beta x_s))\} D = 0 \tag{8}$$

From the above equations, the characteristics equation can be found:

$$C(\gamma, k_s) = \{\frac{L}{2\gamma^2}\{(\cosh(\gamma)$$
$$- \cos(\gamma)) - \frac{k_s L^3}{2EI\gamma^3}[\sinh(\gamma(L-x_s)/L) - \sin(\gamma(L-x_s)/L)]$$
$$\cdot (\cosh(\gamma x_s / L) - \cos(\gamma x_s / L))\} \times$$
$$\frac{L^2}{2\gamma^2}\{(\cosh(\gamma) - \cos(\gamma))$$
$$- \frac{k_s L^3}{2EI\gamma^3}[\cosh(\gamma(L-x_s)/L) - \cos(\gamma(L-x_s)/L)]$$
$$\cdot (\sinh(\gamma x_s / L) - \sin(\gamma x_s / L))\}\} - \{\frac{L}{2\gamma}\{(\sinh(\gamma)$$
$$+ \sin(\gamma)) - \frac{k_S L^3}{2EI\gamma^3}[\cosh(\gamma(L-x_S)/L) - \cos(\gamma(L-x_S)/L)]$$
$$\cdot (\cosh(\gamma x_S / L) - \cos(\gamma x_S / L))\} \times$$
$$\frac{L^3}{2\gamma^3}\{(\sinh(\gamma) - \sin(\gamma))$$
$$- \frac{k_s L^3}{2EI\gamma^3}[\sinh(\gamma(L-x_s)/L) - \sin(\gamma(L-x_s)/L)]$$
$$\cdot (\sinh(\gamma x_s / L) - \sin(\gamma x_s / L))\}\} = 0 \tag{9}$$

where $\gamma = \beta L$ is the normalized wave number or a frequency parameter.

From equation (6), we have

$$EI\beta^4 - \rho A\omega^2 = 0 \qquad (10)$$

Therefore, the relationship between frequency and wave number is given by

$$f = \frac{\gamma^2}{2\pi L^2}\sqrt{\frac{EI}{\rho A}} \qquad (11)$$

The sensitivity of the force sensor beam can be calculated from the frequency. The characteristic equation given by equation (9) defines the wave numbers in terms of k_s. Differentiation of equation (9) with respect to k_s yields

$$\frac{d\gamma}{dk_s} = -\frac{\partial C/\partial k_s}{\partial C/\partial \gamma} \qquad (12)$$

The relationship between frequency f and spring constant k_s can be expressed as

$$\frac{\partial f}{\partial k_s} = \frac{\partial f}{\partial \gamma}\cdot\frac{d\gamma}{dk_s} \qquad (13)$$

Finally, we can obtain the following express

$\frac{df}{dk_s}$ =-(r/π L^2)*(E*I/ρ*A)$^{0.5}$*[(-L^7/8γ^7 EI)*(sinh(γ*(L-x_s)/L)-sin(γ*(L-x_s)/L))*(cosh(γ*x_s/L)-cos(γ*x_s/L))*(cosh(γ)-cos(γ)-(ks*L^3/2EIγ^3)*(cosh(γ*(L-x_s)/L)-cos(γ*(L-x_s)/L))*(sinh(γ*x_s/L)-sin(γ*x_s/L)))-(L^7/8γ^7)*(cosh(γ)-cos(γ)-(ks*L^3/2EIγ^3)*(sinh(γ*(L-x_s)/L)-sin(γ*(L-x_s)/L))*(cosh(γ*x_s/L)-cos(γ*x_s/L)))(1/EI)*(cosh(γ*(L-x_s)/L)-cos(γ*(L-x_s)/L))*(sinh(γ*x_s/L)-sin(γ*x_s/L))+(L^7/8γ^7 EI)*(cosh(γ*(L-x_s)/L)-cos(γ*(L-x_s)/L))*(cosh(γ*x_s/L)-cos(γ*x_s/L))*(sinh(γ)-sin(γ)-(ks*L^3/2EIγ^3)*(sinh(γ*(L-x_s)/L)-sin(γ*(L-x_s)/L))*(sinh(γ*x_s/L)-sin(γ*x_s/L)))+(L^7/8γ^7)*(sinh(γ)+sin(γ)-(ks*L^3/2EIγ^3)*(cosh(γ*(L-x_s)/L)-cos(γ*(L-x_s)/L))*(cosh(γ*x_s/L)-cos(γ*x_s/L)))(1/EI)*(sinh(γ*(L-x_s)/L)-sin(γ*(L-x_s)/L))*(sinh(γ*x_s/L)-sin(γ*x_s/L))/(-(L^4/γ^5)*(cosh(γ)-cos(γ)-(ks*L^3/2EI

$\gamma^{3})*(sinh(\gamma*(L-x_s)/L)-sin(\gamma*(L-x_s)/L))*(cosh(\gamma*x_s/L)-cos(\gamma*x_s/L)))*(cosh(\gamma)-cos(\gamma)$

$-(ks*L^{3}/2EI\gamma^{3})*(cosh(\gamma*(L-x_s)/L)-cos(\gamma*(L-x_s)/L))*(sinh(\gamma*x_s/L)-sin(\gamma*x_s/L)))+(L^{4}/$

$4\gamma^{4})*(sinh(\gamma)+sin(\gamma)+(3ks*L^{3}/2EI\gamma^{4})*(sinh(\gamma*(L-x_s)/L)-sin(\gamma*(L-x_s)/L))*(cosh(\gamma*$

$x_s/L)-cos(\gamma*x_s/L))-(ks*L^{3}/2EI\gamma^{3})*(cosh(\gamma*(L-x_s)/L)*(L-x_s)/L-cos(\gamma*(L-x_s)/L)*(L-x_s)$

$/L)*(cosh(\gamma*x_s/L)-cos(\gamma*x_s/L))-(ks*L^{3}/2EI\gamma^{3})*(sinh(\gamma*(L-x_s)/L)-sin(\gamma*(L-x_s)/L))*(si$

$nh(\gamma*x_s/L)*xs/L+sin(\gamma*x_s/L)*x_s/L))*(cosh(\gamma)-cos(\gamma)-(ks*L^{3}/2EI\gamma^{3})*(cosh(\gamma*(L-x_s)/$

$L)-cos(\gamma*(L-x_s)/L))*(sinh(\gamma*x_s/L)-sin(\gamma*x_s/L)))+(L^{4}/4\gamma^{4})*(cosh(\gamma)-cos(\gamma)-(ks*L^{3}/2$

$EI\gamma^{3})*(sinh(\gamma*(L-x_s)/L)-sin(\gamma*(L-x_s)/L))*(cosh(\gamma*x_s/L)-cos(\gamma*x_s/L)))*(sinh(\gamma)+sin($

$\gamma)+(3ks*L^{3}/2EI\gamma^{4})*(cosh(\gamma*(L-x_s)/L)-cos(\gamma*(L-x_s)/L))*(sinh(\gamma*x_s/L)-sin(\gamma*x_s/L))-($

$ks*L^{3}/2EI\gamma^{3})*(sinh(\gamma*(L-x_s)/L)*(L-x_s)/L+sin(\gamma*(L-x_s)/L)*(L-x_s)/L)*(sinh(\gamma*x_s/L)-si$

$n(\gamma*x_s/L))-(ks*L^{3}/2EI\gamma^{3})*(cosh(\gamma*(L-x_s)/L)-cos(\gamma*(L-x_s)/L))*(cosh(\gamma*x_s/L)*xs/L-co$

$s(\gamma*x_s/L)*x_s/L))+(L^{4}/\gamma^{5})*(sinh(\gamma)+sin(\gamma)-(ks*L^{3}/2EI\gamma^{3})*(cosh(\gamma*(L-x_s)/L)-cos(\gamma*($

$L-x_s)/L))*(cosh(\gamma*x_s/L)-cos(\gamma*x_s/L)))*(sinh(\gamma)-sin(\gamma)-(ks*L^{3}/2EI\gamma^{3})*(sinh(\gamma*(L-x_s)/$

$L)-sin(\gamma*(L-x_s)/L))*(sinh(\gamma*x_s/L)-sin(\gamma*x_s/L)))-(L^{4}/4\gamma^{4})*(cosh(\gamma)+cos(\gamma)+(3ks*L^{3}/$

$2EI\gamma^{4})*(cosh(\gamma*(L-x_s)/L)-cos(\gamma*(L-x_s)/L))*(cosh(\gamma*x_s/L)-cos(\gamma*x_s/L))-(ks*L^{3}/2EI\gamma$

$^{3})*(sinh(\gamma*(L-x_s)/L)*(L-x_s)/L+sin(\gamma*(L-x_s)/L)*(L-x_s)/L)*(cosh(\gamma*x_s/L)-cos(\gamma*x_s/L))-$

$(ks*L^{3}/2EI\gamma^{3})*(cosh(\gamma*(L-x_s)/L)-cos(\gamma*(L-x_s)/L))*(sinh(\gamma*x_s/L)*x_s/L+sin(\gamma*x_s/L)*$

$x_s/L))*(sinh(\gamma)-sin(\gamma)-(ks*L^{3}/2EI\gamma^{3})*(sinh(\gamma*(L-x_s)/L)-sin(\gamma*(L-x_s)/L))*(sinh(\gamma*x_s/L$

)-sin(γ * x_s/L)))-(L^4/4γ^4)*(sinh(γ)+sin(γ)-(ks*L^3/2EIγ^3)*(cosh(γ*(L-x_s)/L)-cos(γ*(L-x_s)/L))*(cosh(γ * x_s/L)-cos(γ * x_s/L)))*(cosh(γ)-cos(γ)+(3ks*L^3/2EIγ^4)*(sinh(γ*(L-x_s)/L)-sin(γ*(L-x_s)/L))*(sinh(γ * x_s/L)-sin(γ * x_s/L))-(ks*L^3/2EIγ^3)*(cosh(γ*(L-x_s)/L)*(L-x_s)/L-cos(γ*(L-x_s)/L)*(L-x_s)/L)*(sinh(γ * x_s/L)-sin(γ * x_s/L))-(ks*L^3/2EIγ^3)*(sinh(γ*(L-x_s)/L)-sin(γ*(L-x_s)/L))*(cosh(γ * x_s/L)* x_s/L-cos(γ * x_s/L)* x_s/L)))]

III. RESULTS DISCUSSIONS

The fabrication processes for the test chip is given in Figure 2. The system parameters used here are as follows: force sensor beam length $L = 500\mu m$; beam Young's modulus $E = 1.3\times10^{11} N/m^2$; beam density $\rho = 2.33\times10^3 kg/m^3$. Once the spring constant is given, the frequency parameter can be found from the characteristic equation. The mode of a beam represents its shape of the vibration. Each mode has a different frequency parameter and has different sensitivity. The sensitivities of the first five modes for the force sensor beam are depicted in Figure 3. From the figure, the odd-order vibration modes were more sensitive than the even-order modes and the first mode was the most sensitive when the spring constant was low. Furthermore, the first mode is most sensitive. When the spring constant, ks, is larger than about $1000 N/m$, the sensitivity of the third mode becomes larger than that of the first mode; and then the beam sensitivity decreases to a maximum value of about $4\times10^{-8} m/N\cdot\sec$. In Figure 4 the sensitivity of mode 1 increased as the length decreased and the spring constant increased.

IV. CONCLUSION

The sensitivity of vibration modes of force sensor beam has been analyzed using The Laplace Transform method. The Results showed that the odd-order vibration modes were more sensitive than the even-order modes and the first mode was the most sensitive when the spring constant was low. Furthermore, the sensitivities of the force sensor beam apparently decreased as the beam length was increased when the spring constant was higher.

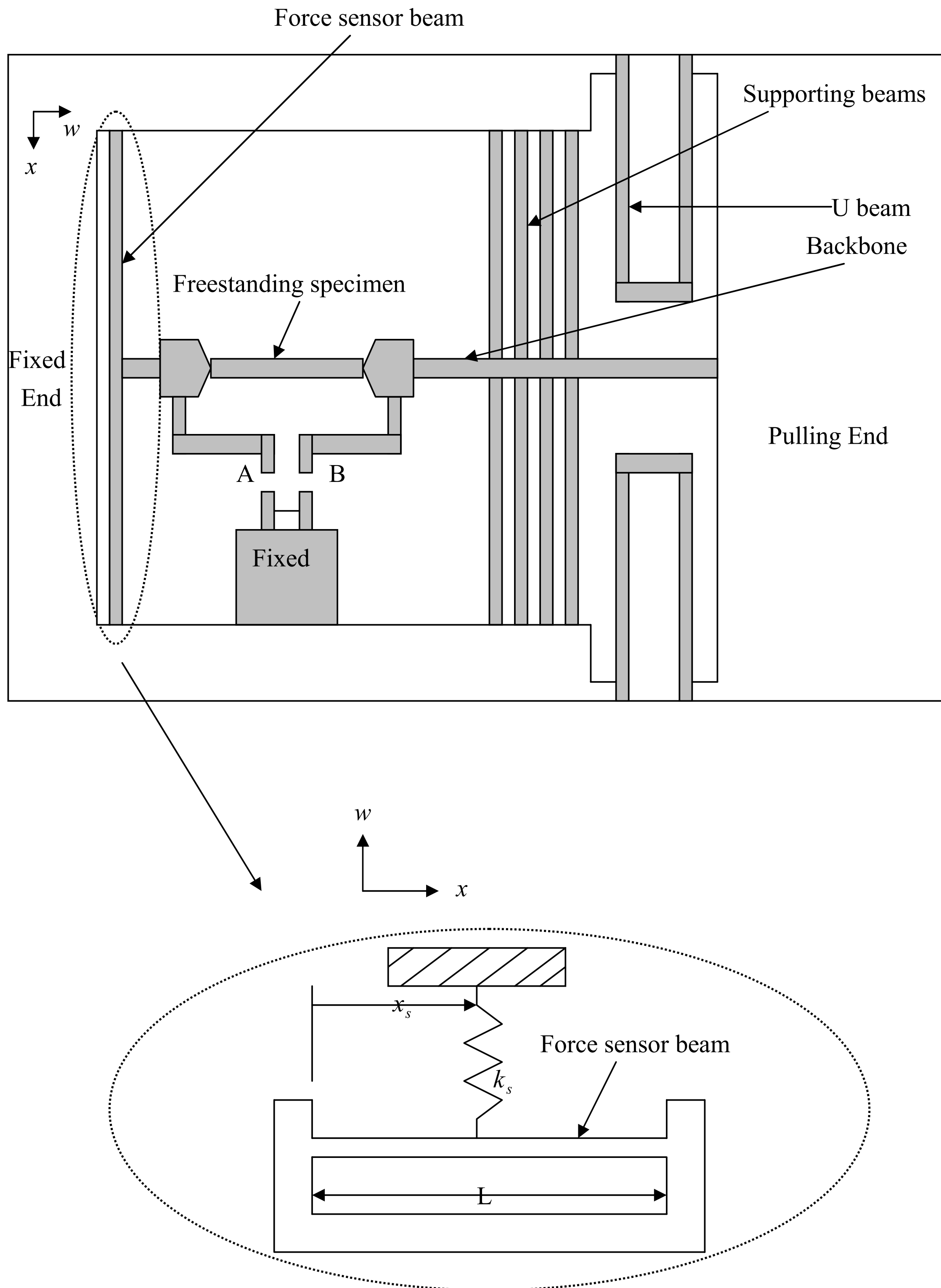

Fig.1. The test chip containing micro-electro-mechanical system force sensor beam.

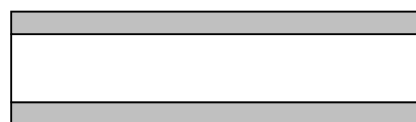

a. Aluminum is sputtered on both sides of wafer with desired thickness.

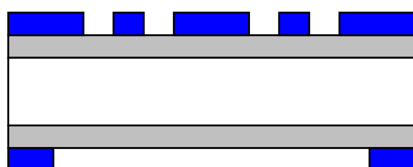

b. The device is patterned on the top , and an etch mask is patterned on the back side of the wafer with photoresist.

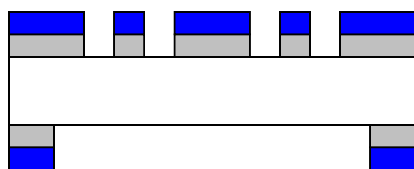

c. Aluminum is etched away on both sides.

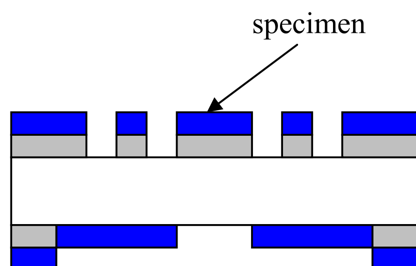

d. Another etch mask, covering only the specimen gauge length only, is patterned on the back side of the wafer.

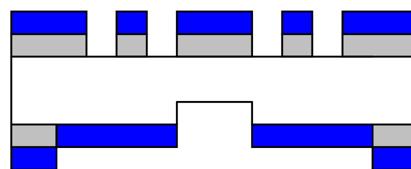

e. Deep reactive ion etching (DRIE) on the back side of the wafer.

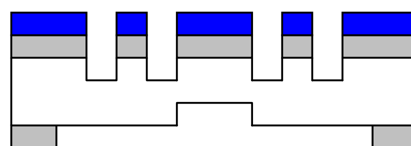

f. Photoresist is removed from the back side of the wafer.

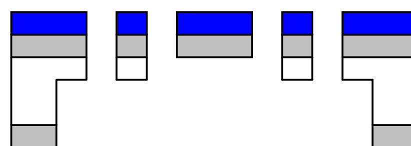

g. DRIE on the top side of the wafer to fabricate the MEMS structures.

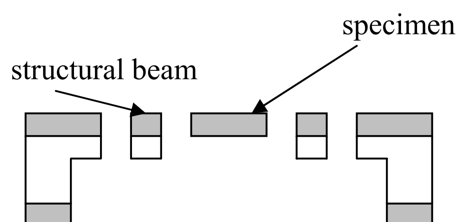

h. Photoresist is removed from the top side of the wafer.

Fig.2. Schematic of the test chip fabrication process.

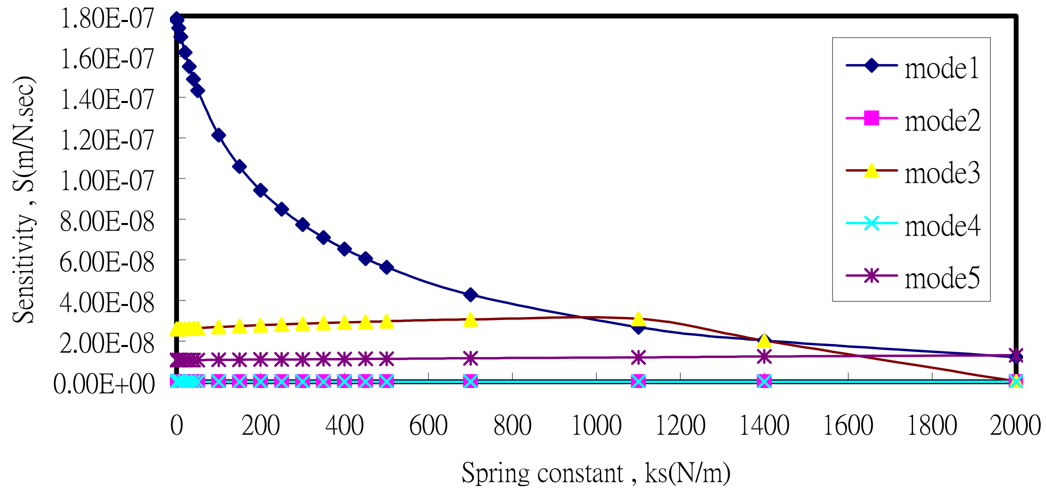

Fig.3. Sensitivity of the force sensor beam versus the spring constant.

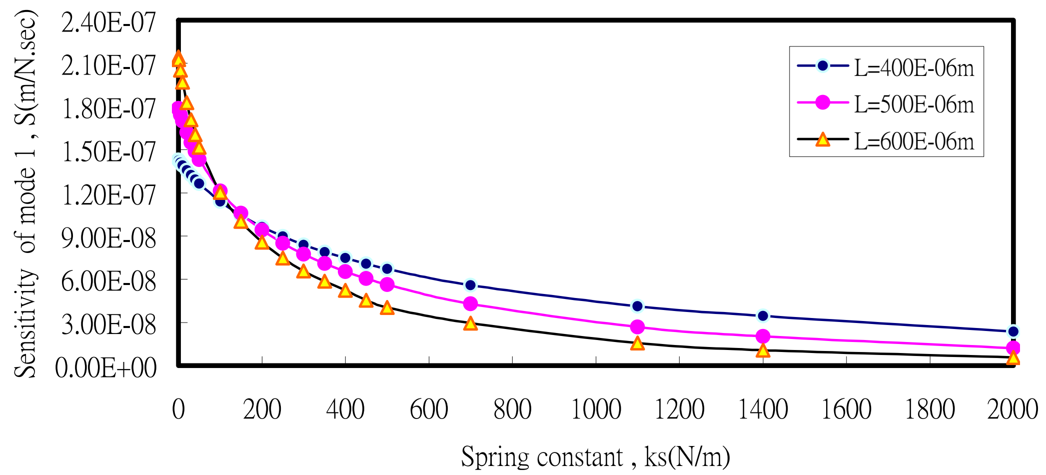

Fig.4. Sensitivity of mode 1 versus the spring constant.

REFERENCES

[1] Majumdar, A., Lai, J., Chandrachood, M., Nakabeppu., O., Wu, Y., and Shi, Z., “Thermal imaging by atomic force microscopy using thermocouple cantilever probes,” Review Science Instrumentation, Vol.66, pp. 3584-3592, 1995.

[2] Rugar, D. and Hansma, P., “Atomic force microscopy,” Physics Today, Vol. 43, pp. 23-30, 1990.

[3] Betzig, E., Finn, P. L., and Weiner, J. S., “Combined shear force and near-field scanning optical microscopy,” Applied Physics Letters, Vol. 60, pp. 2484-2486, 1992.

[4] Simon, A., Brunner, R., White, J. O., Hollricher, O., and Marti, O., “Shear-force distance control at megahertz frequencies for near-field scanning optical microscopy,” Review Science Instrumentation, Vol. 72, pp. 4178-4182, 2001.

[5] Shalom, S., Liebermann, K., Lewis, A., and Cohen, S. R., “A micropipette force probe suitable for near-field scanning optical microscopy,” Review Science Instrumentation, Vol. 63, pp. 4061-4065, 1992.

[6] Haque, M. A. and Saif, M. T. A., “Application of MEMS force sensors for in situ mechanical characterization of nano-scale thin films in SEM and TEM,” Sensors and Actuators A, Vol. 97-98, pp. 239-245, 2002.